

# PRESSURE SENSITIVE PAINTS: FROM LABORATORY TO WIND TUNNEL

**Youssef Mébarki**  
**Institute for Aerospace Research**  
**National Research Council Canada**

**Keywords:** *Pressure Sensitive Paints, PSP, wind tunnel testing*

## Abstract

A research program on Pressure Sensitive Paints (PSP) is underway at the Institute for Aerospace Research of the National Research Council of Canada (NRC). The aim of this program, initiated in the IAR 1.5m x 1.5m Trisonic Blowdown Wind Tunnel is to provide the IAR facilities with an operational PSP technique which is reliable and accurate. The 1.5m pressurized facility poses numerous problems to the PSP technique, such as, pressure sensitivity above ambient pressure and the integrity of optical components subject to high pressure. Therefore, a comprehensive assessment of the PSP system is needed before it is used in a particular facility. This paper presents a description of the IAR laboratory designed to achieve this evaluation. Comparisons of paint performances are given for 5 PSP films all based on a PtFPP porphyrin compound. An example of wind tunnel test preparation on an advanced supercritical transport wing is detailed in the second part of the paper. The effect of the 5 different PSP coatings on the flow at cruise Mach number  $M=0.74$  and three different Reynolds numbers are presented.

## 1 Introduction

The Pressure Sensitive Paint (PSP) technique is an optical method allowing the measurement of surface pressure distribution over a model unlike the conventional sparse pressure tap instrumentation. The phenomenon involved is based on the luminescence of organic compounds quenched by oxygen. When light of appropriate energy excites these molecules, the

emitted intensity is inversely proportional to the air pressure in the medium. For practical application in aerodynamic testing [1], these molecules are embedded in a permeable coating.

Unfortunately, the emission, registered with a scientific CCD camera, will not only depend on the air pressure at the film surface [2]; an assessment of the sensitive film with respect to pressure and temperature is always required. Excitation source stability and proper filter selections can also be critical for accurate PSP measurements in a wind tunnel [3].

Consequently a PSP laboratory was constructed at the IAR, enabling an automated calibration of the coatings versus pressure and temperature. Surface finish analysis of the sensitive films is also available. Our attention will focus herein on five different PSP formulations based on the same sensor: the PtFPP, a photostable Platinum tetra(pentafluorophenyl)porphyrin compound introduced by Khalil et al [4].

The second part of the paper describes an application of the PSP technique to wind tunnel testing in the IAR 1.5m High Speed Wind Tunnel. A prototype half model is tested at the cruise Mach number at three Reynolds numbers. Wind tunnel test section preparation as well as paint application will be discussed. Presented results show the effect of the different coatings on the balance-measured forces.

## 2 The laboratory

### 2.1 Instrumentation

The calibration set up is illustrated in figure 1. The samples under study are placed on a

thermoelectric cooler (TEC), inside a pressure chamber subjected to pressures up to 13.75bar. The pressure controller (PCC200 Scanivalve Corp. pressure) allows for remote control of the pressure in the chamber from 0.01 to 13.75bar. The TEC regulation and stability are guaranteed between 0 and 50°C using a temperature controller (Wavelength Electronics LR3551). The calibrations presented herein are limited from 0.17bar to 2bar and from 10°C to 35°C. Accuracy of the discrete measurements are  $\pm 0.13$ mbar and  $\pm 0.1$ °C. The whole calibration setup remains enclosed to minimize background lighting.

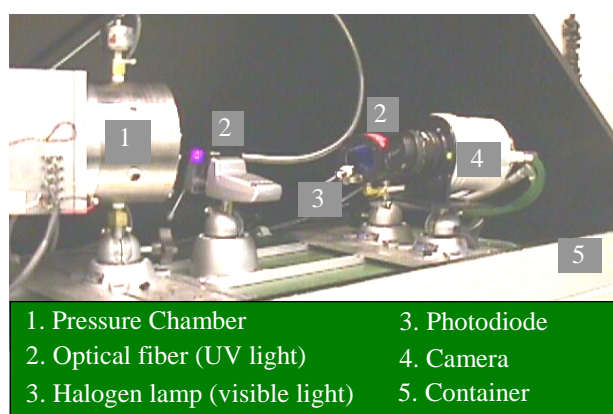


Figure 1: Photography of the PSP calibration setup.

While halogen lamps provide visible excitation, other excitation sources are available. Arc lamps (continuous Mercury and Xenon-Mercury or pulsed Xenon sources) can provide ultraviolet if needed to excite the PSP. A photodiode is placed in the excitation optical path, in order to record the excitation intensity and correct for any drift or sudden changes. Stability analyses have shown that, when properly cooled, the halogen lamp (green Iwasaki JY 1562 GR/N/CG 50W) is very stable with time. It provides minimum drift of the light output: 0.4% per hour, after half an hour warm-up, and significantly less (2x) after one hour warm-up. The level of noise in terms of peak-to-peak fluctuation is 0.02% when averaging the photodiode signal over 200 data-points (at 300Hz). As a comparison, this noise is 20 times less than the one of a stabilized ORIEL 500W

Mercury light source, recorded under the same conditions, and 50 times less than the pulse to pulse repeatability of our Xenon flash lamp (Photogenic PowerLight) operating at full power (1500W). For these reasons, the halogen lamp filtered with a green large band filter (KOPP 4-96) is preferred for the excitation of the porphyrin-based compounds. This compound displays several absorption bands from the ultraviolet to the green and emits strong red phosphorescence (around 650nm) [4], as shown in figure 2. In order to separate completely the emission from the incident light, optical filtering of the signal collected by the camera is needed.

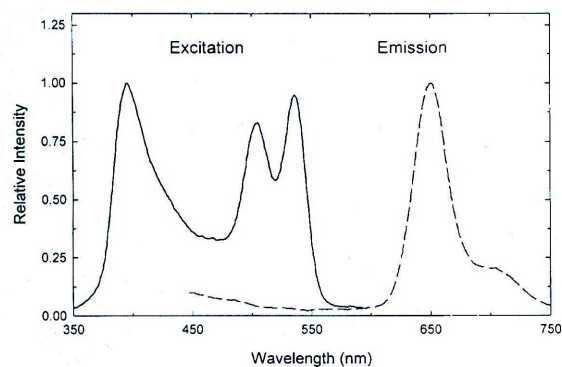


Figure 2: Excitation and emission spectra of the PtFPP molecule.

The minimal spectral leakage from excitation into emission, i.e. optimum pressure sensitivity, is obtained when two interference filters are used in parallel (Andover 650FS40 and Melles Griot 03FIB014) Figure 3 shows the transmittances of the selected reception filters with the excitation large band filter (in blue). Using only the narrow interference filter will reduce the pressure sensitivity of PAR PSP due to spectral leakage with the light source.

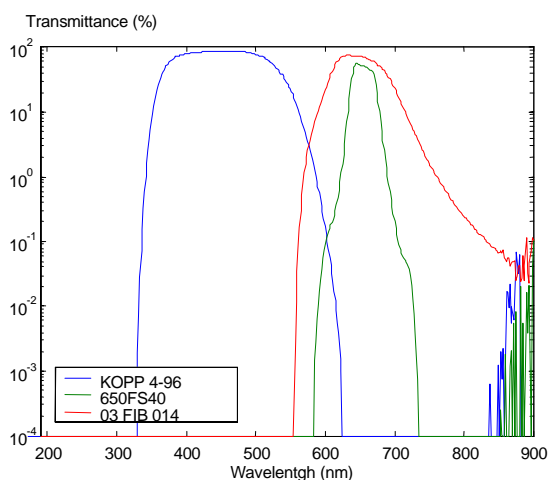


Figure 3: Transmittance of excitation and emission filter used with PtFPP-based sensor and halogen light source.

Two Photometrics 12-bit CCD cameras (512x512 and 1024x1024 pixels) are available for wind tunnel tests. One of the two emission filters is placed inside the selected camera head, behind the camera shutter. Pressure proofing tests have shown that a 6mm thick glass filter can withstand high pressures up to 15bar. This filter therefore protects the vacuum chamber of the CCD from the pressurized environment of the wind tunnel plenum. To meet these specific needs, minor modifications of the camera heads were made by the manufacturer.

## 2.2 Calibration procedure

The software controlling the cameras, called V++, enables script editing using a language called VPascal. The complete automation of the acquisition during a calibration, and eventually during a wind tunnel test, is based upon this ability combined with dynamic data exchange between V++ and Labview programs. In the case of the calibration, a dedicated in-house application, written in Labview, controls and acquires the temperature, the pressure and the photodiode excitation levels for excitation correction. It finally commands V++ to record the PSP emission and perform statistical calculations over the sample of interest (mean value, deviation).

The calibration always starts from the lowest temperature (e.g. 10°C), for which the camera exposure time is determined. Once the targeted temperature is reached and stabilized, a pressure scan is initiated from the lowest to the maximum pressure value. The image acquisition starts only after the pressure is reached with an accuracy of 0.7mbar.

During each pressure scan, lasting from 10min. to 30min. depending on the exposure time, photodegradation of the paint may occur. To detect such an irreversible process, related to destruction of sensitive molecules by the energetic incident light [1], ambient pressure measurements are performed before and after each pressure scan, for each temperature level. The paint stability can therefore be quantified for each temperature level, and further degradation measurements are performed if needed.

As a consequence, large pressure variations will occur at the beginning (e.g. from ambient to 0.17bar) and at the end (e.g. from 2bar back to ambient) of each pressure scan. Because of the response time of PSP coatings to a sudden pressure change, the mean intensity will be measured until equilibrium is reached. Variations of the mean intensity between two measurements must remain within 0.1% of the mean intensity level. This condition must be satisfied 10 times successively, before any data storage.

A complete calibration versus pressure (e.g. 21 points) and temperature (e.g. 7 points) is performed automatically within 2 to 4 hours, once the region of interest on the sample and the appropriate exposure time have been implemented in V++. The dark image is recorded at the end of the calibration before the data storage on disk. Figure 4 shows the computer screen obtained when the calibration is finally completed. Pressure controls (on the right) and temperature controls (on the left) are clearly separated on the screen.

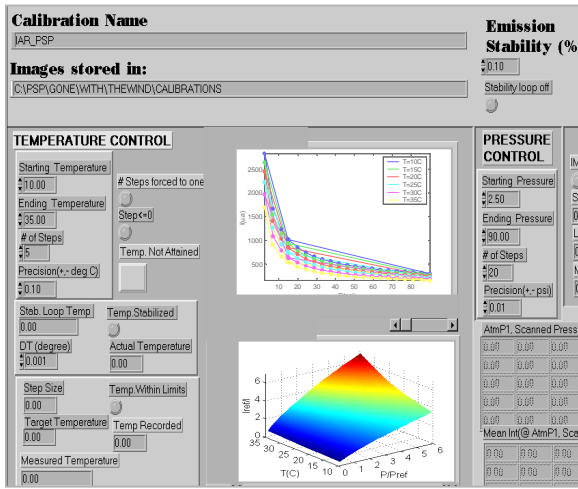


Figure 4: Computer screen of the calibration software (Labview application and Matlab post-processing)

The two figures on the displayed screen correspond to the raw mean intensity versus absolute pressure at different temperatures (upper) and to the surface plot of the intensity ratio versus pressure and temperature (lower). In the former, the noticeable straight lines correspond to the abrupt pressure changes at the beginning and the end of each pressure scan (back to the ambient pressure). For a detailed analysis of such a calibration, the intensity ratio can be expressed as a polynomial function of pressure and temperature. As the inverse relationship is primarily needed in wind tunnel experiments (i.e. the pressure being determined from the measured intensity), the following polynomial interpolation is assumed:

$$\frac{P}{P_{ref}} = \sum_{i=0}^n \sum_{j=0}^m a_{ij} \left( \frac{I_{ref}}{I} \right)^i (T)^j \quad (1)$$

$P_{ref}$ ,  $I_{ref}$ , being the pressure and intensity measurements performed at the reference (wind-off) condition during the calibration: usually ambient temperature and ambient pressure. The error, in terms of the difference between approximation and experimental points, will depend on the values of  $n$  and  $m$ . Figure 5 shows the evolution of the error, when varying the maximum orders  $n$  and  $m$  in equation (1). The approximation was applied to a calibration of the

IAR formulation (PSP PAR) based on PtFPP molecule in silicone polymer.

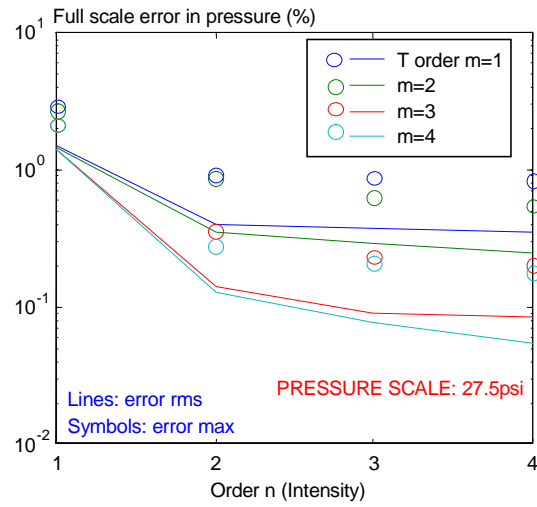


Figure 5: Approximation error of PSP PAR calibration: determination of the maximum orders  $n$  and  $m$  (see eq. 1).

The accuracy of the approximation is slightly improved for orders  $m$  (related to temperature) higher than 2, and no significant improvements are observed for orders higher than  $n=m=3$ . The orders  $m$  and  $n$  are used as well in the inverse of equation (1), relating the intensity ratio to pressure and temperature.

$$\frac{I_{ref}}{I} = \sum_{i=0}^n \sum_{j=0}^m b_{ij} \left( \frac{P}{P_{ref}} \right)^i (T)^j \quad (2)$$

This equation (2) is required to correct from differences between reference conditions in the calibration (noted as  $_{ref}^{ref}$ ) and the wind tunnel experiments (noted as  $_{ref}^{WT}$ ). Indeed, eq. (1) can be rewritten as:

$$\frac{P}{P_{ref}} = \sum_{i=0}^n \sum_{j=0}^m a_{ij} \left( \frac{I^{WT}_{ref}}{I} \frac{I_{ref}}{I^{WT}_{ref}} \right)^i (T)^j$$

The correcting term  $I_{ref}/I^{WT}_{ref}$ , introduced above, is calculated from equation (2) once the reference conditions in the wind tunnel are known. However, the resolution of equation (2) is needed with a good accuracy, only when the *a-priori* calibration [5] is used in wind tunnel testing. The figure 6 shows the approximation of both intensity ratio and pressure (lines)

compared to the experimental data points (circles) for the PSP PAR calibration.

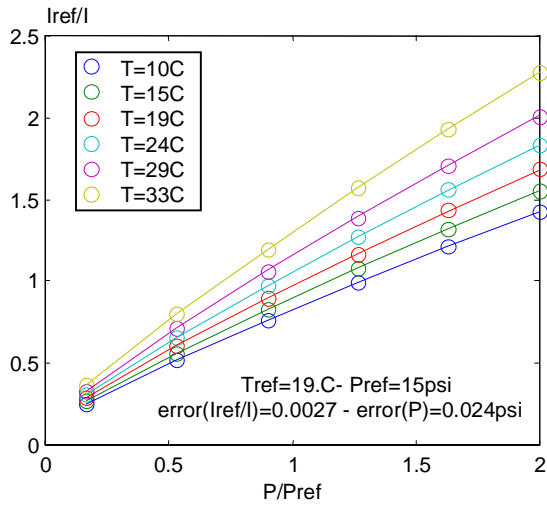


Figure 6: Approximation of PSP PAR calibration:  $n=m=3$  (lines) compared with experimental data points (circles).

### 2.3 Pressure Sensitive Paints

The automated calibration system becomes a necessity when various PSP formulations need to be compared. In preparation for an extensive wind tunnel investigation on different PSP formulations, the setup described above served to characterize pressure and temperature sensitivity of all coatings. In addition to these measurements, roughness measurements were also performed. All PSP formulations under study share one important characteristic: they all used the same porphyrin molecule (PtFPP) as the oxygen sensor. Therefore, the optical system described above (halogen lamp, excitation and reception filters) is suitable for all of these PSP formulations.

Two formulations, one from IAR (noted as PSP PAR), and the PSP FEM developed by Oglesby et al. [6], from NASA LaRC, are not commercially available, while three were supplied by Innovative Scientific Solutions Inc. (ISSI). FIB PSP, initially developed at the University of Washington, as well as the sol-gel PSP and the Uni-Coat PSP are produced commercially by ISSI.

Table 1 details the name, the origin of the PSP used.

PSP	Primer	Ref.	Source
FIB	FIB primer	[7], [8]	ISSI
Sol-gel	ISSI primer	[9]	ISSI
Unicoat	no primer	-	ISSI
FEM	Epoxy Tristar	[6]	NASA LaRC
PAR	Epoxy Tristar	-	IAR

Table 1: PtFPP-based PSP under study

In some cases (PSP FEM, IAR and even FIB), the Tristar (DHMS C4.01TY3) white epoxy primer can be used as the screen layer. Except in the case of the Uni-Coat formulation, which does not require a primer layer, the commercial PSP formulations are supplied with their respective primer. The binder or permeable matrix in which this porphyrin molecule is dissolved will cause different pressure and temperature sensitivities. The pressure sensitivity of the different PSPs are compared in figure 7 for a constant temperature ( $T=T_{ref}=19C$ ). The figure 8 displays the temperature sensitivity measured at ambient pressure for all the PSP under consideration. The temperature sensitivity varies from  $-0.57\%$  per degree for the FIB,  $-1\%$  per degree for the sol-gel, down to  $-1.6\%$  for both FEM and PAR PSP between  $10^{\circ}C$  and  $30^{\circ}C$ .

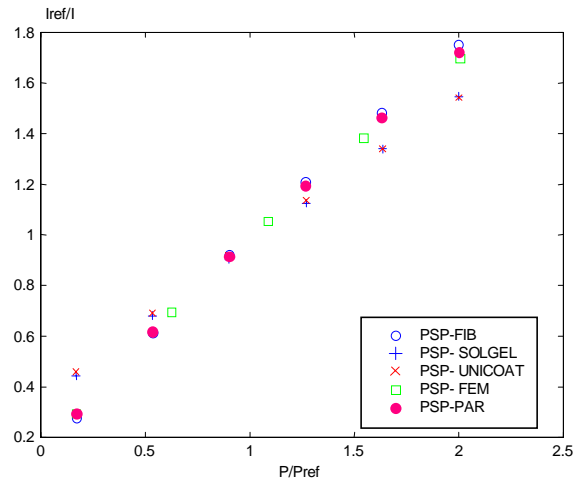


Figure 7: Pressure sensitivity of PtFPP-based formulations at ambient temperature -  $T=T_{ref}=19C$ .

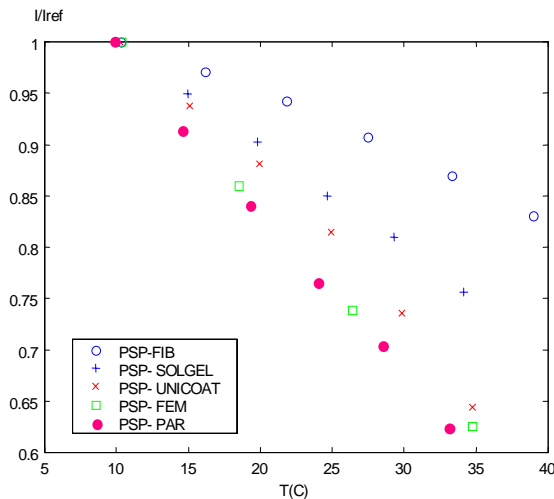


Figure 8: Temperature sensitivity of PtFPP-based PSP around ambient pressure –  $P=P_{ref}=1\text{bar}$ .

The surface roughness of the PSP layers can induce major flow disturbances, causing early transition from laminar to turbulent flow. Previous experiments performed at the Institute for Aerospace Research have shown that PSP coatings on wind-tunnel models can significantly change the performance of the model under study [10]. At transonic speeds, the PSP presence can move the shock forward, causing a severe degradation of the lift performance [7, 11].

The surface quality differences between the PSP formulations arise from the binder chemical composition, the primer surface finish, and the nature of the solvents. The paint application (airbrush settings and appropriate spraying distance and speed) plays an important role on the quality of the final coating. Figure 9 shows the surface finish of samples of commercial PSP, as detected by a Surtronic 3P roughness gauge (given accuracy  $\pm 0.01\mu\text{m}$ ) and recorded by a Labview acquisition program. The maximum average roughness value is obtained for the FIB formulation. It is caused by the  $\text{TiO}_2$  particles used in the FIB primer. A smooth ( $Ra=0.2\mu\text{m}$ ) epoxy primer can reduce the total roughness of the FIB active layer by a factor 2. The sol-gel and Uni-Coat formulations both present low average roughness values (respectively 0.2 and  $0.45\mu\text{m}$ ).

Figure 10 shows that both FEM and PAR present a better surface finish than that of a bare wind tunnel model.

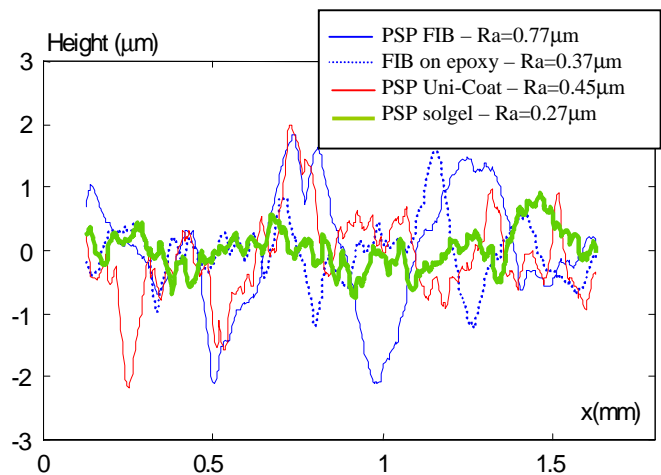


Figure 9: Surface finish of commercial PtFPP- based PSP formulations – Traverse length 1.75mm, cut-off length=0.25mm.

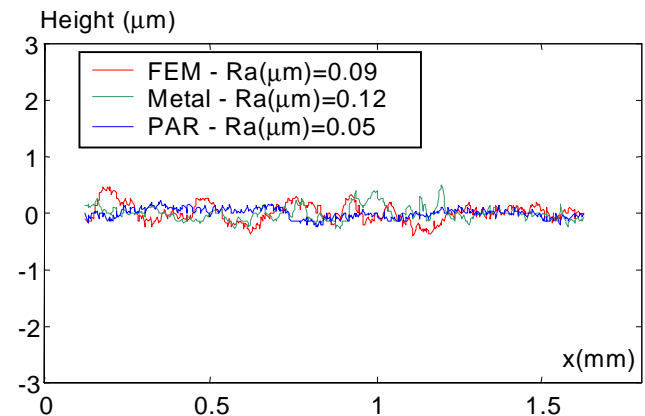


Figure 10: Surface finish of PtFPP- based PSP formulations as compared to bare metal: same condition and same scale as figure 9.

The extremely low value of the PSP PAR formulation was achieved by carefully selecting the solvents (low evaporating rate) and improving the quality of the paint application.

The PSPs evaluated in laboratory are interesting candidates for a wind tunnel evaluation of their performance on the same model geometry. They display different pressure and temperature sensitivities as well as various surface finishes. We propose to analyze the effects of these various coatings on the flow characteristics of a transport aircraft half-model, tested in the Institute for Aerospace Research high-speed facility.

### 3. The wind tunnel

The high speed facility of the Institute for Aerospace Research is a blowdown pressurized wind tunnel operating from low subsonic ( $M=0.1$ ) to supersonic ( $M=4.5$ ). For the current study, tests were performed from  $M=0.2$  to  $M=0.74$  utilizing the 1.5m x 1.5m transonic perforated wall test section. The flow total pressure was varied from 1.23bar to a maximum of 6.2bar, which corresponds to a unit Reynolds number range from 5.6mil/m to 49mil/m.

However, evaluation of the effect of PSP coatings on the flow will only be presented for the cruise Mach number ( $M=0.74$ ) at three Reynolds numbers. The model, shown in figure 11, was originally a twelfth scale version of the Dash 8-100 aircraft. The new supercritical wing, tested without a nacelle, has a 0-degree sweepback measured at the 60% chord line. The wing, made of steel, and the aluminum half fuselage were mounted on the external sidewall balance. The model overall length is 1.73m and its mean aerodynamic chord  $c=0.2$ m. The airfoil sections, used to generate the wing, were designed by de Havilland and IAR to sustain extensive areas of laminar flow with supercritical flow, when boundary layer transition was free. Therefore, to have the wing in its optimum and most sensitive configuration, the half-model is tested in this study with free transition. The wing is equipped with 4 rows of 32 pressure taps. These stations, designated as A, B, C and D, in figure 11, are respectively located at 11%, 27%, 35% and 57% of the wing span (1.1m.).

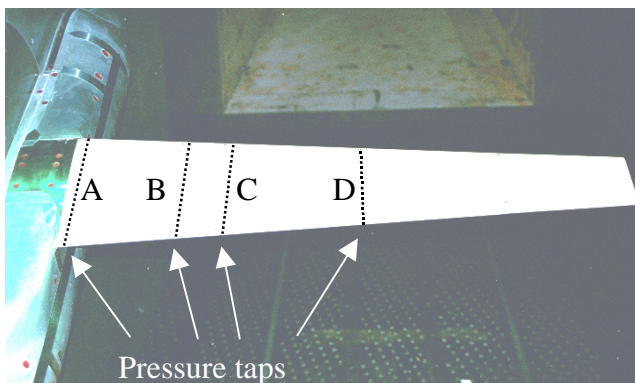


Figure 11: Photograph of the half-model mounted in the test section: wing is coated with the FIB primer.

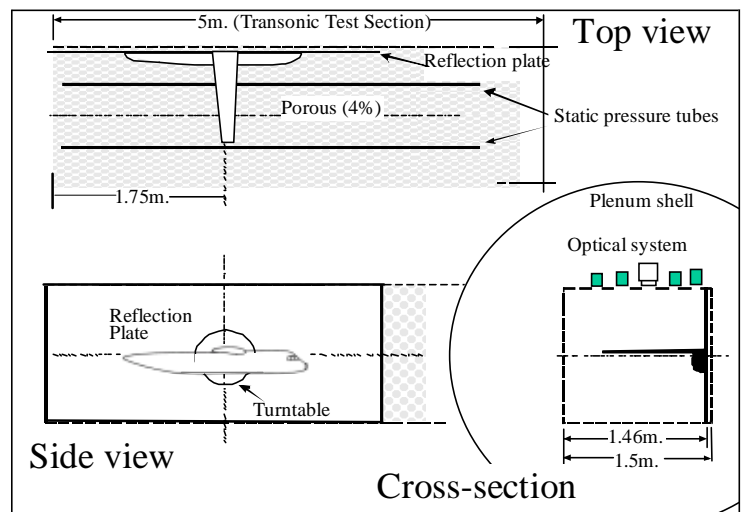


Figure 12: Wind tunnel test section

The half model sidewall balance is used to provide the primary model support and the means of varying the pitch attitude. The total loads for all model components are measured with the 5-component sidewall half-model balance [12]. Figure 12 shows a schematic of the model mounting arrangement in the facility. Two static pressure rails on each wall, except the reflection plate, provide the pressure measurements required for wall correction [13].

The ceiling of the test section is equipped with 20 optical windows. To provide a fairly uniform and stable illumination, 16 filtered and cooled halogen lamps are used. The digital CCD 1024x1024 Photometrics camera and an Infrared Agema 900 camera (136x272 pixels) are also mounted in the plenum shell. The CCD camera records the PSP emission from the wing root (station A) to 85% of the wing span, while the infrared camera focuses on the inner rows of taps: station B and C.

The paint application is performed on both upper and lower wing surfaces in-situ in the wind tunnel test section. Therefore, protection of wind tunnel walls as well as good ventilation is required during this process. Figure 13 shows a photograph of the arrangement including a filtered fan (a), the venting duct (b), the protecting plastic films (c) and an adhesive flooring (d) to ensure maximum cleanliness in the test section.

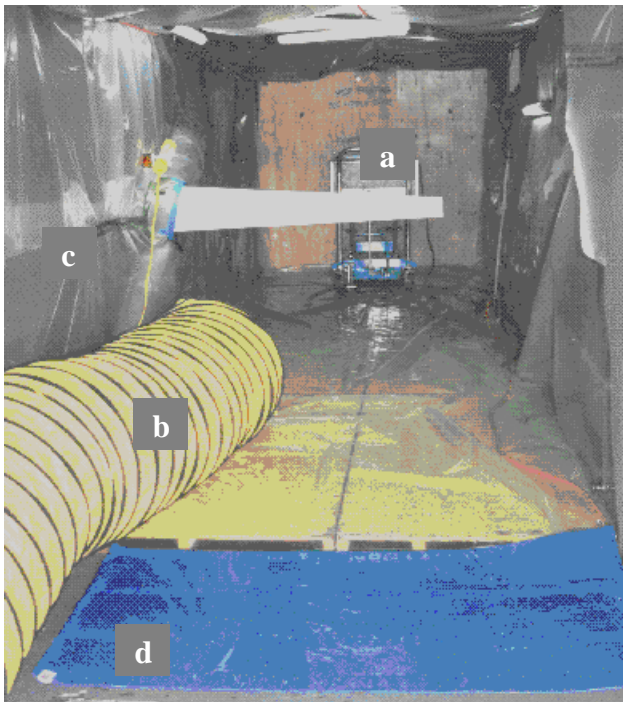


Figure 13: Test section arrangement for PSP application (see text for details).

When a large number of paints are tested, time reduction of the delay between different PSP evaluations is critical. This delay includes model cleaning (from the previous paint), test section protection (20 min), paint application (less than two hours) and paint drying time. Drying time was overnight for most of the coatings and during a weekend for the epoxy primer and the sol-gel formulation. Our newly trained but talented painter applied all the coatings. Two major problems appeared during the paint application. The first concerns the surface finish on the top surface. Painting the leading edge (or even the bottom surface) sometimes lead to accumulation of overspray on the top surface.

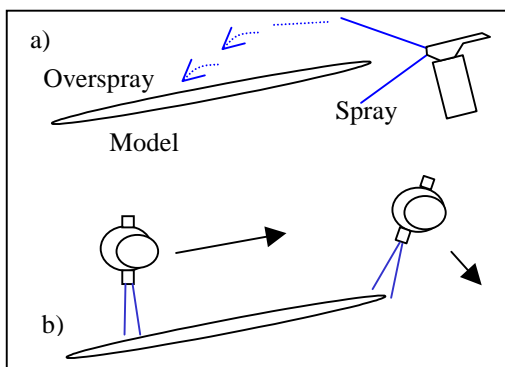


Figure 14: Illustration of the overspray problem (a) and one possible solution (b).

This induces a rough (or dusty) surface if the solvents used evaporate quickly. A solvent with a low evaporating rate enables the extra particles to blend together with the previous coatings (or the next ones). Changing the direction of the application, as shown in figure 14, also improved the top surface finish by reducing the amount of overspray.

The second problem occurred with the FIB primer application. This coating cracked and peeled from the stainless-steel model. A similar problem was previously solved on small coupons by reducing the primer thickness. However, despite several trials (complete cleaning and repeated applications), the FIB primer always fractured at strategic places (near leading edge, flap junctions or pressure tap inserts at leading edge). Because the FIB top-coat is compatible with the robust epoxy primer (which also reduces the FIB roughness), it was decided to apply the FIB active layer on top of the epoxy. The resulting formulation is later referred to as FIBepo.

Table 2 gives the average thickness and roughness measured on the wing for all the tested formulations (thickness gage Positector 6000). For the sol-gel or PAR, the measuring probes were not available and the presented values have been measured later on samples painted concurrently with the model application. For the other coatings, the statistical values are calculated from about 30 measurements distributed over the wing top surface (and only 4 measurements for the bottom surface). When a primer is present, the given thickness is the sum of both the primer thickness (7 $\mu$ m for the sol-gel primer and 25 $\mu$ m for the epoxy primer on the top surface) and the active layer thickness.

PSP	TOP surface e [ $\mu$ m] ( $\sigma$ )	BOTTOM e ( $\mu$ m)	TOP Ra [ $\mu$ m] ( $\sigma$ )	BOTTOM Ra ( $\mu$ m)
Uni-coat	19.7 (7)	10	0.43 (0.1)	0.18
Sol-gel	15 -	-	0.27 -	-
FIBepo	33 (7)	18.5	0.4 (0.05)	0.39
FEM	30 -	21	0.07 (0.02)	-
PAR	29 (5)	-	0.05 (0.01)	-

Table 2: Thickness and roughness measurements on the wing.

The coatings FIBepo, FEM and PAR are applied on the Tristar epoxy primer. Because acetone or toluene does not dissolve this primer, PSP layer cleaning can be performed without removing the epoxy primer layer. A very superficial polishing of the primer (using a polishing paste) is sometimes necessary to remove traces of the previous PSP detected with the CCD camera. As a result, the surface finish of the primer continuously improved with time (from an average roughness of  $0.25\mu\text{m}$  down to  $0.1\mu\text{m}$ ).

Due to inappropriate airbrush settings, the first application of the FEM formulation went on too thick:  $e=45\mu\text{m}$ , including the thickness ( $e=25\mu\text{m}$ ,  $\sigma=5\mu\text{m}$ ) of the primer. As a dramatic consequence, peeling and pitting of the PSP from the leading edge was observed after the first wind tunnel test. Removal of this layer and a second application was performed. The total thickness (primer + active) of the second application was then reduced to  $30\mu\text{m}$ , with a similar surface finish ( $Ra=0.07\mu\text{m}$ ). This thinner FEM coating was able to withstand the flow without damage. A last remark concerns the systematic difference between bottom and top surface in table 2: for practical reasons the bottom surface (not viewed) was always smoother than the top surface (no overspray on the bottom) and generally thinner (no exposure and signal concerns).

### 3.1 Forces measurements

The results are presented, for all the formulations listed in table 2, in terms of balance-measured forces for the cruise Mach number ( $M=0.74$ ). Additional results will be presented elsewhere [14].

During the test, the pitch angle varies continuously from  $\alpha=-4^\circ$  to  $8^\circ$  (uncorrected), at a rate of  $2^\circ/\text{s}$ , while the balance-measured forces are acquired at a  $100\text{Hz}$  frequency. One single data point is the result of the average performed on 25 samples (over  $\Delta\alpha=0.5^\circ$ ). The forces measured on the bare-metal wing (later referred to as “NO PSP” condition) are considered as the reference measurements.

The first result, presented in figure 15, shows the variation of the lift coefficient versus the drag coefficient for the different PSP formulations. The flow conditions are  $M=0.74$  at a Reynolds number based on the mean aerodynamic chord  $Rc=5.7\times 10^6$ .

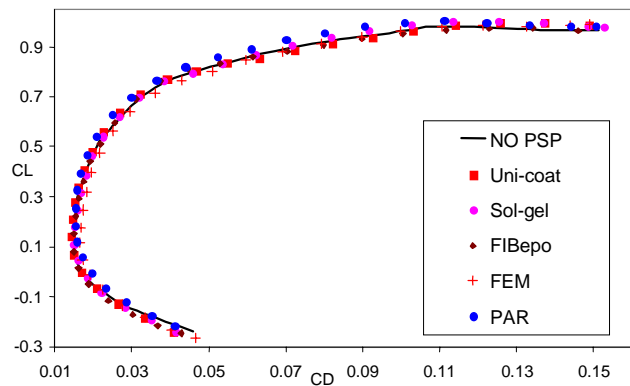


Figure 15: Lift coefficient variation with drag coefficient at  $M=0.74$  –  $R=18.7\times 10^6/\text{m}$  –  $Rc=3.8\times 10^6$ .

Most PSP formulations do not have significant effect on the flow under study, except for the PSP FEM, which induce a reduction of the lift and a drag increase at negative incidences. For the FEM formulation, the drag coefficient at zero lift,  $CD_0$ , increases by 34 drag counts (at  $\alpha=-3.1^\circ$ ), while for the other PSP, it remains within the very good repeatability (1.5d.c.) of the bare wing condition, observed for 3 runs. The lift coefficient reduction at zero angle of attack is 0.089 for FEM, 0.037 for FIB, while for the other PSP it remains below 0.012.

It is interesting to note that the good surface finish of the PAR (twice as good as the bare metal) seems to improve the wing performance only at high angles of attack (between  $2^\circ$  and  $6^\circ$ ). However, the maximum lift, obtained at  $\alpha=6^\circ$  for the clean wing condition (“NO PSP”), is not affected by any of the tested PSPs. Fluorescent oil flow visualizations on the top surface at  $1^\circ$  and  $5^\circ$  have shown that the transition location, actually triggered by the shock (around 50% of the chord), is not affected by the PSP presence.

Force measurements are available for the same Mach number ( $M=0.74$ ) at a higher Reynolds number ( $Rc=5.5\times 10^6$ ), for only two

PSPs: the FIB on epoxy and the Uni-Coat formulations. Figure 16 displays the lift and drag polars obtained for this condition. At negative incidence, a drag increase is observed for the FIBepo only. For example the drag at zero lift condition ( $C_{D0}$  at  $\alpha=-2.88^\circ$ ) is increased by 27 d.c. for the FIBepo and only 5 d.c. for the Uni-Coat. The lift is also significantly reduced by the FIB PSP: at zero incidence the lift coefficient decreases by 0.057 for this formulation (compared to a reduction of 0.019 for the Uni-Coat).

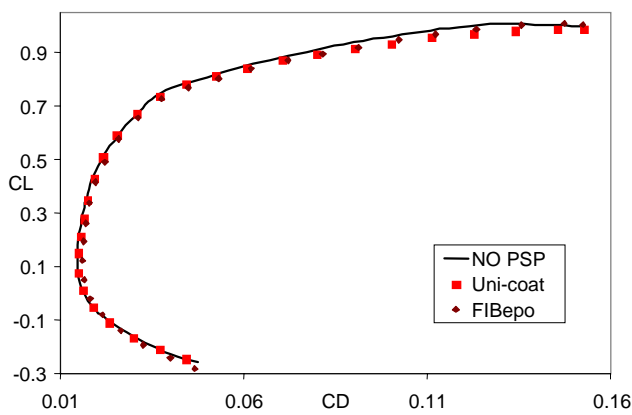


Figure 16: Lift coefficient variation with drag coefficient at  $M=0.74 - R=27.2 \times 10^6/m - R_c=5.5 \times 10^6$ .

The last flow condition presented at the same Mach number ( $M=0.74$ ) is at a greater Reynolds number ( $R_c=8.5 \times 10^6$ ).

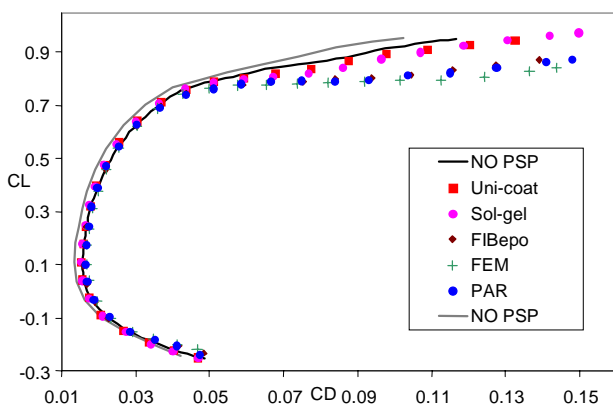


Figure 17: Lift coefficient variation with drag coefficient at  $M=0.74 - R=49 \times 10^6/m - R_c=8.5 \times 10^6$ .

This flow condition is very sensitive to the surface finish: even in the case of bare metal measurements, a good repeatability of the measured forces requires a systematic (and

vigorous) cleaning of the wing between runs. Wing contamination is suspected to trigger the transition earlier. The two NO PSP measurements given in figure 17 represent the two extreme NO-PSP-forces among the 5 repeat runs performed during the whole test program ( $\Delta C_L \sim 0.03$  and  $\Delta C_D \sim 10 \text{ d.c.}$ ) at this condition.

All PSP formulation measurements agree very well with one of the two bare wing measurements, only for angles of attack below  $2.5^\circ$ . Above this limit, two behaviors are observed: the Uni-Coat and sol-gel PSP both remain close to the NO PSP conditions, whereas the three other PSPs show a significant decrease of the maximum lift. This result, totally unexpected for the smooth FEM and PAR formulations, is very interesting since the FIBepo, being 10 times rougher than the PAR, induces similar effect on the flow.

Schairer et al. [11] have already noted that smooth PSP coatings ( $Ra=0.5$  to  $0.75 \mu\text{m}$ ) on a supercritical semi-span wing shifted the shock wave location upstream. This roughness height being submerged in the viscous sub-layer of a developed turbulent boundary layer, it satisfies the criterion of “hydraulically smooth” surface ( $k^+ = Ra \cdot u_\tau / \nu < 5$ ) and the authors suspected the PSP thickness to change the shape of the profile.

To investigate the effect of the PSP coating thickness on our supercritical wing, a very thin and smooth ( $e=3.75 \mu\text{m}$ ,  $Ra=0.04 \mu\text{m}$ ) PAR active layer was applied directly on the bare wing after the epoxy removal.

The result, compared in figure 18 with the thicker PAR PSP (active + primer) and the best NO PSP forces previously presented, shows that the large reduction of lift observed at high angles of attack is not due to the coating thickness. This result was confirmed for the thick ( $45 \mu\text{m}$ ) FEM first application, which compared well with the second thin ( $30 \mu\text{m}$ ) FEM film.

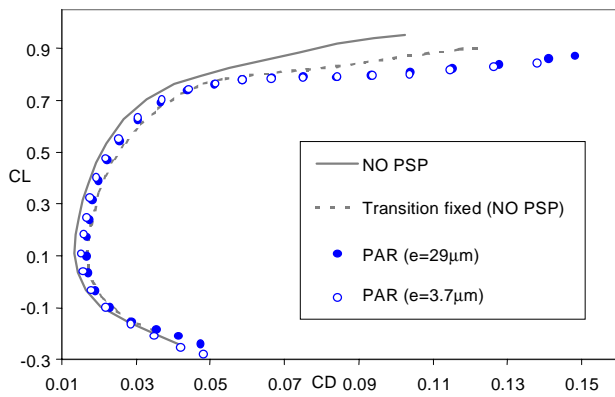


Figure 18: Effect the coating thickness on the wing at  $M=0.74 - R=49 \times 10^6/m - R_c=8.5 \times 10^6$ .

From fluorescent oil visualizations performed at this flow condition on the bare metal wing, it was observed that the transition location is far from the leading edge at  $1^\circ$  (around 40% chord). Thus, the transition fixing (at 15% chord on both surfaces) on the bare metal wing significantly reduces the wing performance [15], as illustrated in figure 18. It is interesting to note that the PSP effect on the flow appears to be slightly less (or equal in the case of the thick coating) than that of the transition fixing at angles of attack below  $2.5^\circ$ . For greater incidences, the wing performance with PSP becomes lower, which indicates that the transition with PSP is occurring near the leading edge (before the first 15% of the chord).

#### 4 Discussion

Two of the PSPs presented in this study, the PSP PAR and FEM, have exceptional surface qualities (hardly reached in wind tunnel model machining). Also, the comparison of the intrusiveness of various PSP coatings has shown that the roughness (when expressed as an average) and the film thickness are not the predominant source of flow perturbation, within the present range of thickness and roughness.

Future work will focus on extensive surface assessments of all the tested PSP formulations (2D spatial analysis, maximum peak-to-peak depth...), in order to understand the good results of the relatively rough Uni-Coat. However, another explanation can be derived from the observation of the two behaviors mentioned earlier (see figure 17):

three PSP induce similar effect on the flow while two others (sol-gel and Uni-Coat) have very little effect on the flow at high angles of attack, high Reynolds number.

Similarly, in figure 7 showing the pressure sensitivity of all coatings, two trends can as well be observed: both Uni-Coat and sol-gel (falling on the same line) have lower pressure sensitivity than the three others. Because the same sensor is used in all these formulations, this can be caused by a different permeability of the PSP binders.

How can the PSP permeability affect the boundary layer development?

Permeability is related to the free volume available in the polymer film, which in turn can result in reducing the paint hardness. In that case, a plausible explanation could be a local PSP deformation (exceeding the PSP roughness by several orders of magnitude) at the stagnation point, for the highest Reynolds number.

Permeability as well as quantitative hardness measurements of the PSP coatings should be available in the near future. Nevertheless, it is believed that film softness might not be accountable for the observed results, for two reasons: softer than steel, the PSP PAR and FEM were found to be as hard as the Uni-Coat (according to the fingernail scratching test).

The second reason emerged during the test, when performing oil flow visualization on FEM, FIB and PAR coatings. While a thin film of oil on the bare metal wing does not affect the flow, it was found, with some surprise, that the presence of oil on the PSP surface improves the results at the highest Reynolds number.

To evaluate the influence of oil, additional experiments have been performed at this sensitive flow condition. In figure 19, the transition free bare-metal measurements are reported with and without a thin oil film at the first 10% of the chord (top and bottom surfaces). They are compared with the PAR (29µm thick) with and without oil around the first 10% of the chord (LE stands for leading edge in figure 19).

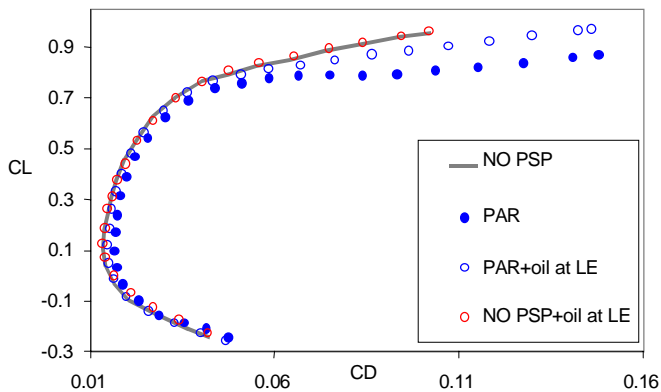


Figure 19: Effect of a thin film of oil on the PSP performance -  $M=0.74$  -  $R=49 \times 10^6/m$  -  $R_c=8.5 \times 10^6$ .

The film of fluorescent oil was so thin that it barely flowed during the wind tunnel test. However, the oil significantly increased the maximum lift and the wing performance is then very close to the one obtained for Uni-Coat or sol-gel on the wing (see figure 17). Because traces of oil have no impact on the PSP softness, it is unlikely that the difference in the PSP hardness is the cause for the degradation of the lift performance.

On the other hand, the oil film has a noticeable effect on the PSP surface tension and further investigations (surface tension effect on transition location) might be of interest. In any case, the sensitivity of an advanced supercritical wing to the surface quality, especially near the leading edge, can be fully appreciated.

## 5 Conclusion

Different PSP formulations were compared using a fully automated calibration system. Assessment of the surface finish for various coatings was completed prior to wind tunnel application on a supercritical wing. The effect of PSP coatings on the wing performance was analyzed at the cruise Mach number ( $M=0.74$ ) for three Reynolds numbers. At the highest Reynolds number tested ( $R_c=8.5 \times 10^6$ ), it was observed that the smoothest and thinnest PSP films were causing a significant lift reduction at high angles of attack above  $2.5^\circ$ .

## Acknowledgments

Special thanks are due to the IAR High Speed Facility Operating and Instrumentation Groups, and in particular to Michel Grenier, who provided dedicated support at every stage of the PSP development and implementation in wind tunnel. The author wishes to express his gratitude to Don Oglesby and Jeffrey Jordan, from NASA LaRC, for kindly providing us the FEM formulation and to Richard Poole, formerly of de Havilland (Toronto), for his support and assistance during the test.

## References

- [1] McLachlan BG and Bell JH. *Pressure Sensitive Paint in Aerodynamic Testing*, Experimental Thermal and Fluid Science, Elsevier Science Inc., 1995.
- [2] Shanze KF, Carroll BF, Korotkevitch S and Morris MJ. *Temperature Dependence of Pressure Sensitive Paints*, AIAA Vol. 35-2, 1997.
- [3] Hand A L. *Control of Spectral Leakage in Luminescence measurements*, 7<sup>th</sup> Annual Pressure Sensitive Paint Workshop, Purdue University, October 1999.
- [4] Khalil GE, Gouterman MP and Green E. *Method and sensor for measuring oxygen concentration*, US Patent 5,043,286, Aug.1991.
- [5] Shimbo Y, Noguchi M and Makino Y. *Blowdown tunnel application of pressure sensitive paint*, AIAA, Reno, AIAA-99-3169, 1999.
- [6] Oglesby D and Upchurch B. *In pursuit of the ideal pressure sensitive paint*, 7<sup>th</sup> Annual Pressure Sensitive Paint Workshop, Purdue University, October 1999.
- [7] Sellers ME. *Pressure Sensitive Paint data on the Transonic Technology Demonstrator (TST) in the AEDC Propulsion Tunnel 16T*, Final Report AEDC TR-98-3, 1998.
- [8] Ruyten W and Fisher CJ. *On the effects of reflected light in luminescent paint measurements*, AIAA 2000-0833, 2000.
- [9] Jordan DJ, Watkins N, Davis PN, Weaver WL, Dale GA, Navarra KR, Urban JR, Devoid E and Strange RA. *Pressure sensitive paint measurement in the large-scale commercial engine-test stand*. ICIASF conference proceedings, Toulouse, 1999.
- [10] Mébarki Y, Grenier M and Mokry M. *Mutual Effects of Air Flow and Pressure Sensitive Paint in a Wind Tunnel*, 46<sup>th</sup> CASI conference, 7<sup>th</sup> Aerodynamic Symposium, Montreal, 1999.

- [11] Schairer ET, Metha R.D., Olsen ME, Hand LA, Bell JH, Whittaker PJ and Morgan DG. *The effects of Thin Paint Coatings on the Aerodynamics of semi-Span Wings*, AIAA, Reno, AIAA 98-0587, 1987.
- [12] Brown D. *Information for users of the National Research Council's 5-dtx5-ft blowdown wind tunnel at the National Aeronautical Establishment 3<sup>rd</sup> ed.*, NRC Laboratory technical report LTR-HA-6, 1977.
- [13] Mokry M, Khalid M and Mébarki Y, *The art and science of wind tunnel wall interference: new challenges*, ICAS 2000 Congress, Harrogate, 2000.
- [14] Mébarki Y, Grenier M and Thain J, *Pressure sensitive paint application on a supercritical wing at cruise speeds*, International Symposium on Flow Visualization, Edinburgh, 2000.
- [15] Poole R., *Drag reduction and advanced supercritical wings at cruise speeds, report on the phase 2 test period*, de Havilland, DHC-ISTC-97-1, 1997.